

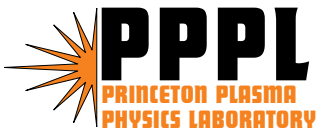
PPPL-4121

PPPL-4121

The Role of Aspect Ratio and Beta in H-mode Confinement Scalings

S.M. Kaye, M. Valovic, A. Chudnovskiy, J.G. Cordey, D. McDonald,
A. Meakins, K. Thomsen, R. Akers, G. Bracco, et al.

October 2005



Prepared for the U.S. Department of Energy under Contract DE-AC02-76CH03073.

Princeton Plasma Physics Laboratory

Report Disclaimers

Full Legal Disclaimer

This report was prepared as an account of work sponsored by an agency of the United States Government. Neither the United States Government nor any agency thereof, nor any of their employees, nor any of their contractors, subcontractors or their employees, makes any warranty, express or implied, or assumes any legal liability or responsibility for the accuracy, completeness, or any third party's use or the results of such use of any information, apparatus, product, or process disclosed, or represents that its use would not infringe privately owned rights. Reference herein to any specific commercial product, process, or service by trade name, trademark, manufacturer, or otherwise, does not necessarily constitute or imply its endorsement, recommendation, or favoring by the United States Government or any agency thereof or its contractors or subcontractors. The views and opinions of authors expressed herein do not necessarily state or reflect those of the United States Government or any agency thereof.

Trademark Disclaimer

Reference herein to any specific commercial product, process, or service by trade name, trademark, manufacturer, or otherwise, does not necessarily constitute or imply its endorsement, recommendation, or favoring by the United States Government or any agency thereof or its contractors or subcontractors.

PPPL Report Availability

Princeton Plasma Physics Laboratory

This report is posted on the U.S. Department of Energy's Princeton Plasma Physics Laboratory Publications and Reports web site in Fiscal Year 2006.

The home page for PPPL Reports and Publications is:

http://www.pppl.gov/pub_report/

Office of Scientific and Technical Information (OSTI):

Available electronically at: <http://www.osti.gov/bridge>.

Available for a processing fee to U.S. Department of Energy and its contractors, in paper from:

U.S. Department of Energy
Office of Scientific and Technical Information
P.O. Box 62
Oak Ridge, TN 37831-0062

Telephone: (865) 576-8401

Fax: (865) 576-5728

E-mail: reports@adonis.osti.gov

The Role of Aspect Ratio and Beta in H-mode Confinement Scalings

S.M. Kaye¹, M. Valovic², A. Chudnovskiy³, J.G. Cordey², D. McDonald², A. Meakins², K. Thomsen⁴, R. Akers², G. Bracco⁵, C. Brickley², C. Bush⁶, A. Cote⁷, J.C. DeBoo⁸, M. Greenwald⁹, G.T. Hoang¹⁰, D. Hogweij¹¹, F. Imbeaux¹⁰, Y. Kamada¹², O.J.W.F. Kardaun¹³, A. Kus¹³, S. Lebedev¹⁴, V. Leonov³, S. Lynch¹⁵, Y. Martin¹⁶, Y. Miura¹², J. Ongena¹⁷, G. Pacher⁷, C.C. Petty⁸, M. Romanelli⁵, F. Ryter¹³, K. Shinohara¹², J. Snipes⁹, J. Stober¹³, T. Takizuka¹², K. Tsuzuki¹², H. Urano¹²

¹ Princeton Plasma Physics Laboratory, Princeton University, Princeton NJ, USA

² UKAEA Association Euratom, Culham, UK

³ Nuclear Fusion Inst., Russian Research Center Kurchatov Inst., Moscow, RUSSIA

⁴ EFDA, Garching, GERMANY

⁵ Associazione Euratom-ENEA sulla fusione, Frascati, ITALY

⁶ Oak Ridge National Laboratory, Oak Ridge TN, USA

⁷ Centre Canadien de Fusion Magnetique, Varennes, Quebec, CANADA

⁸ General Atomics, San Diego CA, USA

⁹ MIT Plasma Science and Fusion Center, Cambridge MA, USA

¹⁰ Association Euratom-CEA, CEA de Cadarache, St. Paul lez Durance, FRANCE

¹¹ FOM Instituut voor Plasmafisica, Rijnhuizen, Nieuwegein, NETHERLANDS

¹² Naka Fusion Res. Establishment, Japan Atomic Energy Res. Inst., Naka, JAPAN

¹³ Max-Planck Institut fur Plasmaphysik, Garching, GERMANY

¹⁴ A.F. Ioffe Institute, Russian Academy of Sciences, St. Petersburg, RUSSIA

¹⁵ Dept. of Sociology, Princeton University, Princeton, NJ, USA

¹⁶ EPFL/CRPP Association Euratom, Lausanne, SWITZERLAND

¹⁷ LPP,ERM-KMS, Association EURATOM-Belgium State, Brussels, BELGIUM

E-mail: skaye@pppl.gov

Abstract. The addition of high power, low aspect ratio data from the NSTX and MAST experiments have motivated a new investigation of the effect of aspect ratio on confinement scaling. Various statistical methods, including those that incorporate estimates of measurement error, have been applied to datasets constrained by the standard set of criteria in addition to the range of κ and M_{eff} appropriate to ITER operation. Development of scalings using engineering parameters as predictor variables results in ϵ -scaling coefficients that range from 0.38 to 1.29; the transformation of these scalings to physics variables results in an unfavorable dependence of B_T on β , but a favorable dependence on ϵ . Because the low aspect ratio devices operate at low B_T and therefore high β_T , a strong correlation exists between ϵ and β , and this makes scalings based on physics variables imprecise.

1. Introduction

Recent analysis of the international H-mode confinement database focused on extracting the dependence of the thermal confinement ($\tau_{E,\text{th}}$) on beta (β) and collisionality (ν_*) through the use of a variety of statistical methods [1]. In particular, it was shown that in an extreme case, the data could be consistent with a null dependence on β , in line with results from dedicated scans on DIII-D and JET [2,3], rather than a strongly unfavorable dependence such as in the IPB98(y,2) scaling [4]. One of the important aspects of this work was the use of statistical methods in which the measurement error of the predictor (“independent”) and response (dependent) variables could be included in the analysis. The use of this approach coupled with the more standard ones led to a range of parametric dependences that fit the data well.

The objective of the present paper is to study the role of aspect ratio (R/a) and beta on confinement by making use of the high power, low aspect ratio data recently contributed to the database from the NSTX and MAST devices. While some of this data was in the analysis in

[1], there were too few observations to conduct a precise study of their effect on the scalings. Both NSTX and MAST operate at aspect ratios of $R/a=1.3$ to 1.5 , a factor of approximately two lower than that of ITER and most of the data in the H-mode database. In addition, both devices operate in a range of elongation (1.6 to 2.4) that encompasses the ITER target operating point, making the study of the aspect ratio effect relevant to the ITER shape. Prior to the inclusion of the low aspect ratio data, the dependence of confinement with this parameter was obtained from a dataset extending only to higher aspect ratio (up to 5.5), but with this high aspect ratio data provided by devices with cross-sectional shapes dissimilar from that of ITER. Both PDX and ASDEX operated near $R/a=4$, but with circular cross-sections, and PBX-M ran at $R/a=5.5$, but with indented, or “bean-shaped”, plasmas.

In this work, the role of aspect ratio on governing confinement trends will be examined by comparing results from a variety of statistical methods as applied to datasets with different constraints. These methods include Ordinary Least Squares Regression (OLSR), a Bayesian approach [5,6], and the Principal Component Error-In-Variable (PCEIV) technique used in recent analyses [1,7]. The latter two techniques take measurement error of the variables into account. Because the low aspect ratio devices operated at vacuum toroidal fields (B_T) that are an order of magnitude lower than those of conventional aspect devices, and therefore higher β_T ($=\langle p \rangle / (B_T^2 / 2\mu_0)$), a significant correlation exists between β and ϵ (the inverse aspect ratio, $\epsilon=a/R$, will be used as a predictor variable rather than aspect ratio itself). This makes a precise determination of the ϵ and β dependence difficult.

In Section 2, a description of the new data and analysis selection criteria, along with the statistics and condition of the selected datasets will be given. Results of the statistical analysis will be given in Section 3, and an extrapolation of the results to ITER and to a Component Test Facility (CTF) based on a low aspect ratio design [8] will be given in Section 4.

2. Data and Selection Criteria

2.1 NSTX

NSTX operates with $a=0.67$ m and $R=0.85$ m ($R/a=1.27$). Over 90 H-mode discharges from the 2002 to 2004 experimental campaigns were contributed to the international H-mode confinement database. The discharges were sawtooth-free, they were both ELM-free and ELMy with either Type I or smaller ELMs, and they exhibited periods of stationary stored energies for at least several energy confinement times. The parameter ranges of the data are $I_p=0.6$ to 1.2 MA, $B_T=0.3$ to 0.5 T, line-averaged density= 1.5 to 7×10^{19} m⁻³, elongation $\kappa=1.7$ to 2.4 , and with D^0 neutral beam injection, with thermal power loss $P_{L,th}$ from 1.9 to 7.1 MW at beam energies up to 100 keV, into D^+ plasmas. Plasma operation was in either Double Null (DN) or Lower Single Null (SNL) divertor configurations; the SNL configuration had the ion grad-B drift in the favorable direction. The NSTX data exhibited enhancement factors of 0.6 to 1.4 relative to the IPB98(y,2) scaling, and while the data scaled nearly linearly with I_p at fixed B_T , the data statistically exhibited a weaker I_p and stronger B_T dependence than that given by this scaling, with $\tau_{E,th} \sim I_p^{0.5} B_T^{-1}$ [9, 10].

2.2 MAST

The MAST data represent quasi-stationary ELMy plasmas with and without sawteeth. The dataset covers the engineering parameter range of $I_p=0.73$ to 0.78 MA, $R_{geo} = 0.8$ to 0.83 m, $a=0.54$ to 0.57 m ($R/a=1.47$), $\kappa=1.9$ to 2.0 , triangularity $\delta=0.44$ to 0.52 , $B_T=0.45$ to 0.49 T, line averaged density $n_e=3.0$ to 5.4×10^{19} m⁻³ and $P_{L,th}=1.5$ to 2.4 MW. All data were from a double null divertor configuration. The working gas was deuterium and plasmas were heated with neutral beams with energy 40 keV. Typically, one of the two beam lines was operated in hydrogen to improve the ion temperature measurement, but the amount of hydrogen from the single beam was small, and $M_{eff}=1.94$ to 2.0 , as confirmed by neutral particle analyser measurements. The effective charge measured by bremsstrahlung emission at mid radius was

$Z_{\text{eff}}=1.1$ to 1.4. The thermal energy confinement time on MAST broadly agrees with the IPB98(y,2) scaling. It is observed, however, that the plasmas with lower collisionality have better confinement normalized to IPB98(y,2) than high collisionality plasmas [11].

2.3 Data Selection

The data to be used for this study come from the ITPA confinement database DB4V2, which is based on the now public DB3V13 but with the addition of 92 NSTX, 7 MAST and 507 JET datapoints. The data selected for this study were constrained first by the standard selection, which, among other criteria, is based on limiting fast ion content and ensuring near-stationary conditions [1 and references therein]. Furthermore, for this study whose aim is to isolate the effect of aspect ratio, the data were constrained to both elongation and M_{eff} ranges from 1.6 to 2.4. The effect of shaping on the β -dependence is studied in [12]. The number of observations satisfying these constraints for each tokamak are: ASDEX-U (509), C-Mod (31), COMPASS (16), DIII-D (264), JET (1487), MAST (9), NSTX (53), PBX-M (36) and START (7). The weighting of the data for each tokamak to be used in the subsequent statistical analyses is $w_j=1/N_j^{1/2}$, where N_j is the number of observations for the j^{th} tokamak. This weighting, is different from the $1/(2+N_j^{1/2}/4)$ weighting used in [1] and references therein, in which the effect from tokamaks with the greatest number of observations still dominate. At another extreme, a $1/N_j$ weighting would treat the data from each machine equally. While we adopt the compromise $1/N_j^{1/2}$ weighting, results from the other two weightings will be discussed. Measurement errors for the engineering parameters are as in [1, 7]: $\delta I_p=1.3\%$, $\delta B_T=1.5\%$, $\delta n_e=5\%$, $\delta P=14\%$, $\delta R=1.3\%$, $\delta \epsilon=3.2\%$.

The addition of the low aspect ratio data in the ITPA database extends the range of both β and ϵ significantly. This is shown in Fig. 1, where $\beta_{\text{th,TOT}}$ is plotted as a function of ϵ for the set of data satisfying the above constraints. Here, $\beta_{\text{th,TOT}}$ is the thermal pressure normalized to the total magnetic field, defined as $B_{\text{TOT}} = [B_T^2 + B_{\text{pol}}^2]^{1/2}$, where B_T is the vacuum toroidal field at the geometric axis and B_{pol} is the poloidal field determined from q_{95} . This value of the magnetic field is used in the calculation of the dimensionless parameters since, in a low aspect ratio device, $B_{\text{pol}} \sim B_{\text{tor}}$ at the plasma edge, and thus the poloidal field influences the plasma beta and normalized gyroradius ρ_* ($\sim T_e^{1/2}/\epsilon R B_{\text{TOT}}$). Furthermore, use of the total magnetic field is consistent with the Troyon definition of β [13]. For the low aspect ratio devices, the difference between the toroidal, B_T , and the total magnetic field, B_{TOT} can be up to 25%.

As can be seen in Fig. 1, the addition of MAST and NSTX extend the range of $\beta_{\text{th,TOT}}$ by a factor of approximately five, and the range of ϵ by over a factor of two. In principle, this should help improve the determination of the scaling with these parameters. However, as is seen in the figure, and as was pointed out in [11], the fact that the higher ϵ devices operate at higher β introduces a strong correlation between these two parameters. It is also seen that the lower ϵ PBX-M data is at higher $\beta_{\text{th,TOT}}$ as well, due to operation in its indented configuration. It will be seen that including PBX-M data in this analysis will reduce the favorable ϵ dependence for a given β dependence. The NSTX and MAST data lie in a collisionality regime that is well within the range of data at lower ϵ , but at 50% higher ρ_* due to operation at low B_T .

Examples of how well previously published thermal confinement scalings describe the ϵ dependence are shown in Fig. 2. Fig. 2a shows the thermal confinement enhancement factor H as a function of ϵ for the IPB98(y,2) scaling, while Fig. 2b shows the H -factor relative to the scaling given in Eq. 9 of [1], where the confinement is taken to scale as β^0 . The IPB98(y,2) scaling goes as $\epsilon^{0.58}$ when expressed in engineering variables, while the scaling given in Eq. 9 of [1] goes as $\epsilon^{0.39}$. In both cases, the scalings overpredict the confinement time for high ϵ data (NSTX, MAST and START), as indicated by $H < 1$ for these scalings for those devices. Similar results are found for the other scalings presented in [1].

To perform the statistical analyses, two sets of predictor variables are chosen; engineering (I_p , B_T , n_e , R , $P_{L,th}$ and ϵ), and physics (ρ_* , β , v_* , q and ϵ). B_T is used in the engineering variable fits since use of B_{TOT} would lead to a coupling of this parameter with I_p . The physics variables are defined with respect to volume-averaged values of thermal plasma density, total magnetic field and q_{cyl} . The engineering variables show some significant pairwise correlations among the variables. The most significant correlations in the dataset that includes PBX-M are between I_p/R , $I_p/P_{L,th}$ and $R/P_{L,th}$. In the dataset without PBX-M, the correlation between B_T/ϵ is also high, reflecting the correlation between β and ϵ seen in Fig. 1. The correlations for both datasets are given in Table 1.

Table 1. Pairwise correlations for the κ -1.6-2.4, $M_{eff}=1.6$ -2.4 dataset with (red) and without (black) PBX-M. The strongest correlations are denoted by the bold/italicized font.

	$\ln I_p$	$\ln B_T$	$\ln n_e$	$\ln R$	$\ln P$	$\ln \epsilon$
$\ln I_p$	1	0.50	-0.04	0.82	0.86	0.31
$\ln B_T$	0.49	1	0.43	0.48	0.40	-0.84
$\ln n_e$	-0.02	0.43	1	-0.33	-0.01	-0.17
$\ln R$	0.74	0.48	-0.33	1	0.77	-0.59
$\ln P$	0.83	0.41	0.00	0.77	1	-0.28
$\ln \epsilon$	0.01	-0.63	-0.12	-0.48	-0.14	1

Using the physics variables as a predictor set introduces the issue that several of them are functions of the same variables, such as stored energy, ϵ and q (e.g., $\rho_* \sim W^{1/2}/\epsilon$, $\beta \sim W$, $v_* \sim q/(\epsilon^{3/2}W^2)$, $q \sim \epsilon^2$). Consequently, correlations in the variables and their errors emerge in part due to these common factors. Using the definitions of the physics variables given in [4], significant correlations exist between ρ_*/ϵ , β/ϵ and ρ_*/β , and even in a “reduced” set, with the common factor of stored energy normalized out [1], correlations still exist between v_*/ρ_* , v_*/β and ϵ/β .

3. Statistical Results

Three statistical analysis methods have been used to analyze the confinement trends. Ordinary Least Squares Regression (OLSR) is a standard technique that is used with the underlying assumption that the principal measurement error is in the response variable. The Principal Component Error-In-Variable (PCEIV) method was employed in [1] to account for errors. In this approach the principal components (PC) of the logs of the predictor and response variables normalized by their errors are computed. A PC with a zero eigenvalue gives an exact linear relation among the variables. The minimum eigenvalue in practice is not zero, but it is small and is related to the scatter of the data about the PC. For this PC, then, the eigenvalue is assumed to be zero in order to determine this linear relation.

Finally, a Bayesian analysis is used [5,6]. Bayesian inference explicitly uses probability models to quantify data uncertainties and to fit the data. In this first application of this approach to this confinement data, we assume that the predictor variables are uncorrelated and that their actual value for each observation is assumed to be within a normal distribution centered about the measurement. The width of the normal distribution is such that 99% of all possible values are contained within three standard deviations of the measured value. The three standard deviations constitute the measurement error. The value of the dependent variable is also assumed to be within a normal distribution, but with unknown error (i.e., large variance). A log-linear model was assumed for the fit, and the data were not weighted. Future studies using this method will focus on varying the models and the assumptions within the models.

In order to develop the range of scalings for discharge shapes similar to that of ITER, the dataset without PBX-M will be used as a base case. The OLSR for this dataset, with the datapoints weighted as described in Sec. 2, yields the following relation:

$$\tau_{E,th} = 6.25e-10 I_p^{0.80} B_T^{0.32} n_e^{0.39} R^{2.12} P_{L,th}^{-0.66} \epsilon^{0.94} \quad (1)$$

in units of sec, A, T, m⁻³, m and W. This is similar to the IPB98(y,2) scaling but with a stronger ϵ dependence ($\tau \sim \epsilon^{0.58}$ in IPB98(y,2)). When transformed to physics variables, Eq. 1 can be expressed as:

$$B_T \tau \sim B_T^{0.03} \rho_*^{-2.86} \beta_T^{-0.70} v_*^{-0.09} q^{-2.26} \epsilon^{0.62} \quad (2)$$

exhibiting an unfavorable dependence on β , and a weaker explicit dependence on ϵ than when expressed in terms of the engineering variables. The normalized confinement also exhibits a favorable dependence with decreasing q . The small residual dimensional dependence ($B^{0.03}$) indicates that the scaling nearly satisfies the Kadomtsev constraint (B^0 in this description). A comparison among the different methods is given in Tables 2a and 2b. Table 2a shows the results based on the engineering predictor variables, while the first five rows of Table 2b show these results when transformed to physics variables. The last three rows of Table 2b show results using the reduced physics variables as the predictor set. For all cases except for case 3, the measurement errors among the variables are assumed to be uncorrelated. Correlated errors do exist, however, for certain variables such as ϵ ($=a/R$) and B_T ($=B_0 R_0/R$, where the subscript '0' refers to the value at the center stack). These correlated errors can be taken into account using the PCEIV method, and the results based on them are given as PCEIV-C (case 3) [14].

The Root Mean Square Error is defined as $RMSE = \sqrt{\frac{\sum_{i=1}^N (y_{exp} - y_{fit})^2}{(N-2)}}$, where y_{exp} is the natural log of the experimental value and y_{fit} is that of the value from the scaling.

Table 2a: $\tau_{E,th}$ Scaling coefficients for the engineering predictor variables for three different statistical techniques. The uncertainties in the exponents are shown for the OLSR and Bayesian cases.

Case		Coeff	I_p	B_T	n_e	R	$P_{L,th}$	ϵ	RMSE
1	OLSR	6.25e-10	0.80	0.32	0.39	2.12	-0.66	0.95	0.166
			± 0.02	± 0.02	± 0.01	± 0.03	± 0.01	± 0.06	
2	PCEIV	1.02e-9	0.66	0.42	0.42	2.28	-0.64	1.29	0.172
3	PCEIV-C	9.43e-10	0.73	0.36	0.39	2.14	-0.62	1.03	0.169
4	Bayesian	3.40e-9	0.96	0.16	0.30	1.83	-0.67	0.38	0.160
			± 0.03	± 0.03	± 0.02	± 0.07	± 0.01	± 0.10	
5	OLSR-NBI only	4.78e-9	0.83	0.29	0.34	2.05	-0.68	0.76	0.160
			± 0.02	± 0.02	± 0.01	± 0.04	± 0.01	± 0.06	

The tables indicate a range of scalings and ϵ dependences, depending on which method is used. In Table 2a, the ϵ dependence determined by the OLSR, PCEIV and PCEIV-C methods are stronger, and more favorable for low aspect ratio, than those in IPB98(y,2) or the scalings determined in [1]. PCEIV-C gives a scaling with a slightly weaker ϵ dependence than PCEIV, and an interplay between I_p and B_T is also seen by comparing cases 2 and 3. The Bayesian approach gives the weakest ϵ dependence and the lowest RMSE. This approach, however, does not weight the datapoints, and thus the result is biased towards the devices with the largest number of datapoints (JET, DIII-D and ASDEX-U). Indeed, when different weightings are used, different scaling results are obtained. As examples, using the $1/(2+N_j^{1/2}/4)$ weighting from [1], which does not de-emphasize the larger data contributions as much as $1/N_j^{1/2}$, OLSR

Table 2b: $B_{TOT}\tau_{E,th}$ scaling coefficients for the physics variables. The first four rows are the coefficients determined from the transformation of the results for the engineering variables given in Table 2a, and the last three rows are the results using the reduced physics variables (i.e., stored energy normalized out of all except β) as predictor variables.

Case		Coeff	ρ_*	β	v_*	q_{cyl}	ϵ	RMSE
1a	OLSR		-2.86	-0.70	-0.09	-2.26	0.62	
2a	PCEIV		-2.93	-0.51	-0.10	-1.73	0.61	
3a	PCEIV-C		-2.78	-0.48	-0.12	-1.80	0.33	
4a	Bayesian		-2.67	-1.01	-0.11	-2.80	0.27	
5a	OLSR-NBI		-2.73	-0.96	-0.10	-2.49	0.44	
5	OLSR	2.40e-7	-2.28	0.19	-0.36	-0.32	-1.68	0.308
6	PCEIV	6.48e-8	-2.72	-0.14	-0.18	-0.95	-0.37	0.396
7	Bayesian	4.85e-7	-2.16	0.17	-0.40	-0.39	-1.58	0.303

yields

$$\tau_{E,th} \sim I_p^{0.85} B_T^{0.27} n_e^{0.35} R^{2.01} P_{L,th}^{-0.66} \epsilon^{0.73} \quad (3)$$

while weighting each tokamak equally (i.e., through a $1/N_j$ weighting), OLSR gives

$$\tau_{E,th} \sim I_p^{0.70} B_T^{0.44} n_e^{0.44} R^{2.32} P_{L,th}^{-0.68} \epsilon^{1.35} \quad (4)$$

The influence of NSTX, with its weaker I_p dependence, is seen in (4) as the influence of this device is increased. Note also the stronger ϵ dependence. Case 5 is an OLSR result when the standard dataset is constrained to discharges that are heated only by neutral beam injection. The fit is similar to that in Case 1, although with a weaker dependence on ϵ . OLSR scalings with elongation included, where $\tau_{E,th}/\kappa^\alpha$, $\alpha=0.5, 0.75$ and 1.0 , result in scalings with similar RMSEs as Case 1 and, as an example, for $\alpha=1.0$, the coefficients for $(I_p, B_T, n_e, R, P_{L,th}, \epsilon)$ become $(0.76, 0.41, 0.41, 2.20, -0.71, 1.06)$.

When transformed to physics variables, all the scalings based on the engineering variable predictor set shows an unfavorable scaling on β . The ρ_* and ϵ -dependences, when transformed from engineering variables, are sensitive to several of the engineering variable dependences, specifically those of n_e, R and $P_{L,th}$. Using the OLSR result (Eq. 1) as an example, when the engineering coefficients are varied within their uncertainties (see Table 1), the transformations to physics variables leads to the following ranges:

$$B\tau \sim \rho_*^{-(2.67-3.04)} \beta^{-(0.59-0.82)} v_*^{-(0.06-0.13)} q^{-(2.14-2.39)} \epsilon^{(0.43-0.81)}$$

The scalings based directly on the reduced physics parameter predictor set (Cases 5 to 7) indicate a weak dependence on β , but an unfavorable dependence on ϵ . The dependence on v_* , however, is more favorable than that in the transformations from the engineering variable scalings (i.e., higher $B\tau$ for lower v_*). The fits based on the physics parameters, however, are poor (in terms of the RMSE metric), due to correlations among the variables and their errors. The systematic differences in the β and ϵ dependences between the engineering and the reduced physics variable scalings result also from the differences in the dependent variable used for these scalings (i.e., P instead of τ or W_{th}). This will be discussed in more detail in [12]. These physics variable scalings, therefore, are shown for comparison purposes and will not be used for predictions. Fits based on the engineering variables (cases 1 and 3) are shown in Fig. 3. Also shown is the $\tau_{E,th}^{exp}/\tau_{E,th}^{fit}$ as a function of ϵ for the scalings.

The influence of PBX-M can be assessed by determining the scaling with the data for this device included. Using the PCEIV method as an example, the resulting scaling is

$$\tau_{E,th} \sim I_p^{0.90} B_T^{0.13} n_e^{0.31} R^{1.77} P_{L,th}^{-0.55} \epsilon^{0.21} \quad (5)$$

exhibiting a stronger I_p , weaker B_T and a much weaker ϵ dependence when compared to the results for Case 2. The latter is due to the relatively higher β and τ of PBX-M at the lowest ϵ , possibly due to its indented shape. We also note that excluding data from the low power, small, low aspect ratio device START has an insignificant impact on the scalings in the dataset with no PBX-M data.

In addition to the range of scaling coefficients that result from applying different statistical techniques, the precision of the estimates with respect to the measurement errors can be assessed. An illustration of this is shown in Fig. 4, where the range of coefficients obtained when the errors on W_{th} and $P_{L,th}$ were varied by +/-50% are plotted. The red shaded region shows the range of power and ϵ coefficients (α_p , α_ϵ), while the blue shaded region shows the range of β and ϵ coefficients resulting from the transformation from engineering to physics variables. The diamonds show the values of the coefficients for the experimental measurement error (14% for both W_{th} and $P_{L,th}$). Clearly seen is the interplay between the β and ϵ exponents, indicative of their correlation.

4. Summary and Predictions

The addition of high power, low aspect ratio data from the NSTX and MAST experiments have allowed for an investigation of the effect of aspect ratio on confinement scaling. Various statistical methods, including those that incorporate estimates of measurement error, have been applied to datasets constrained by the standard set of criteria in addition to the range of κ and M_{eff} appropriate to ITER operation. Development of scalings using engineering variables as the predictor set results in ϵ -scaling coefficients that range from 0.38 to 1.29; the transformation of these scalings to physics variables results in unfavorable dependences on β . Because the low aspect ratio devices operate at low magnetic field and high β_T , a strong correlation exists between ϵ and β , making scalings based on physics variables unreliable.

No one scaling expression that can be identified as the “best scaling” emerges from this analysis; consequently, the scalings developed here can be used as a set to estimate only a range of possible confinement times for future devices. This is done for both ITER and a low aspect ratio design for a Component Test Facility (CTF) [8], and the results are given in Table 3. Two confinement estimates are given for ITER, one for the base case ($\beta_T \sim 2.6\%$), where the loss power is held constant at 87 MW, and one for an enhanced performance case, where the loss power was adjusted in order for $\beta_i=4\%$, as was done in [1]. No M_{eff} corrections were made to the estimates since the M_{eff} dependences, as determined in [1], were weak. Three methods (cases 1, 2 and 3) show similar confinement predictions for the base case of ITER, while the scaling based on NB-only data (Case 5) is lower. The β -degradation in all these scalings result in much lower confinement estimates at $\beta_i=4\%$.

The confinement estimates for the CTF are based on the lowest divertor power flux case given in [8]. Because the CTF operates at higher elongation than ITER ($\kappa=3.2$), a correction factor of $(3.2/2)^{0.75}$, consistent with the scalings developed in [1], was applied to the confinement estimates. For CTF, a confinement time of 0.32 s is required to meet its objectives. The confinement estimates based on Cases 1 to 3 indicate that a confinement enhancement factor of approximately two (over these H-mode scaling estimates) is necessary. CTF, however, may operate in a hot ion mode in which the ion transport would be close to neoclassical levels while the electron transport would be dominant. In this case, the confinement time for CTF would be greater than those given by the predictions in Table 3 [8].

Additional data from the low aspect ratio devices, including those from dedicated β -scans and from aspect ratio similarity experiments, will help further refine the β and ϵ -dependences

reported here. In particular, data from low aspect ratio plasmas with $\beta_{th,TOT}$ values that overlap those from conventional aspect ratio would help improve the condition of the database. This can be accomplished by running either low input power, low R/a plasmas, or low B_T , high input power plasmas at higher aspect ratio.

Table 3: Energy confinement time predictions for ITER and CTF

Case	Predictor Variables	Method	ITER ($\beta_r \sim 2.6\%$)	ITER ($\beta_t = 4\%$)	CTF
1	Engineering	OLSR	3.47 s	1.33 s	0.16 s
2	Engineering	PCEIV	3.46	1.41	0.15
3	Engineering	PCEIV-C	3.46	1.56	0.16
5	Engineering	OLSR-NBI	3.16	0.89	0.14

Acknowledgments A portion of this work was supported by US DOE Contract DE-AC02-76CH03073.

References

- [1] Cordey, J.G. et al., *Nuc. Fusion*, **45** (2005) 1078.
- [2] Petty, C.C., Luce et al., *Phys. Plasmas* **11** (2004) 2514.
- [3] McDonald, D.C. et al., *Plasma Phys. Controlled Fusion* **46** (2004) A215.
- [4] ITER Physics Basis, *Nuc. Fusion* **39** (1999) 2137.
- [5] Gelman, A. Carlin, J., Stern, H. and Rubin, D., *Bayesian Data Analysis 2nd Ed.* (Boca Raton:, Chapman & Hall/CRC)
- [6] Dose, W., W. Von Der Linden an dA. Garrett, *Nucl. Fusion* **36** (1996), 735.
- [7] Thomsen, K et al., *Analysis of the bias in H-mode confinement scaling expressions related to measurement errors in variables*, (Proc. 31st EPS Conference on Plasma Physics, London, 2004) ECA Vol. 28G, Paper P5.145
- [8] Peng, M., *A Component Test Facility based on the Spherical Tokamak* (to appear in Proc. 32nd EPS Conference on Plasma Physics, Tarragona, 2005).
- [9] Kaye, S.M. et al., *Progress Towards High Performance Plasmas in the National Spherical Torus Experiment (NSTX)* accepted for publication in *Nuc. Fusion* (2005).
- [10] Kaye, S.M. et al., *Energy confinement scaling in the Low Aspect Ratio National Spherical Torus Experiment (NSTX)*, in preparation (2005).
- [11] Valovic, M. et al., *Nucl. Fusion* **45** (2005) 942.
- [12] Takizuka, T., Urano, H., Takenaga H., Oyama, N., *Origin of the various beta dependence of ELMy H-mode confinement properties*, this conference.
- [13] Troyon, F., Gruber, R., Saurenmann, H., Semenzato, S., Succi, S., *Plasma Physics and Controlled Fusion* 1984 **26** 209.
- [14] Fuller, W.A., *Measurement Error Models*, Wiley and Sons, 1987.

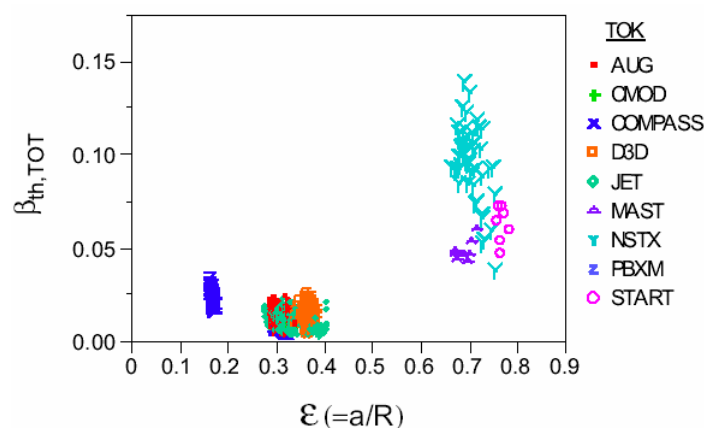


Fig. 1 Range of $\beta_{th,TOT}$ and ϵ (inverse aspect ratio) from the constrained ITPA H-mode database.

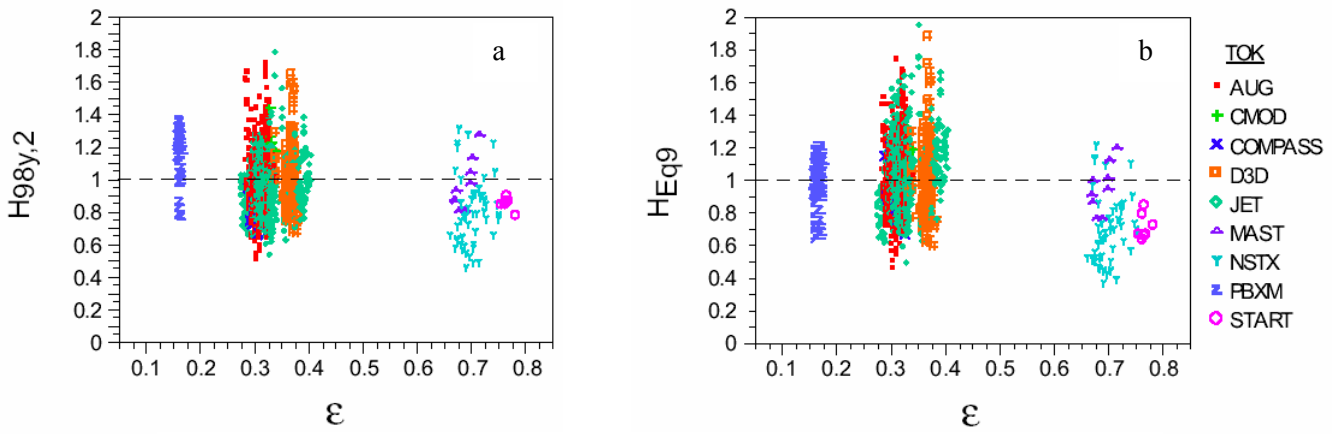


Fig. 2 Confinement enhancement factor as a function of inverse aspect ratio for the IPB98(y,2) scaling (a) and from Eq. 9 in Reference 1 (b).

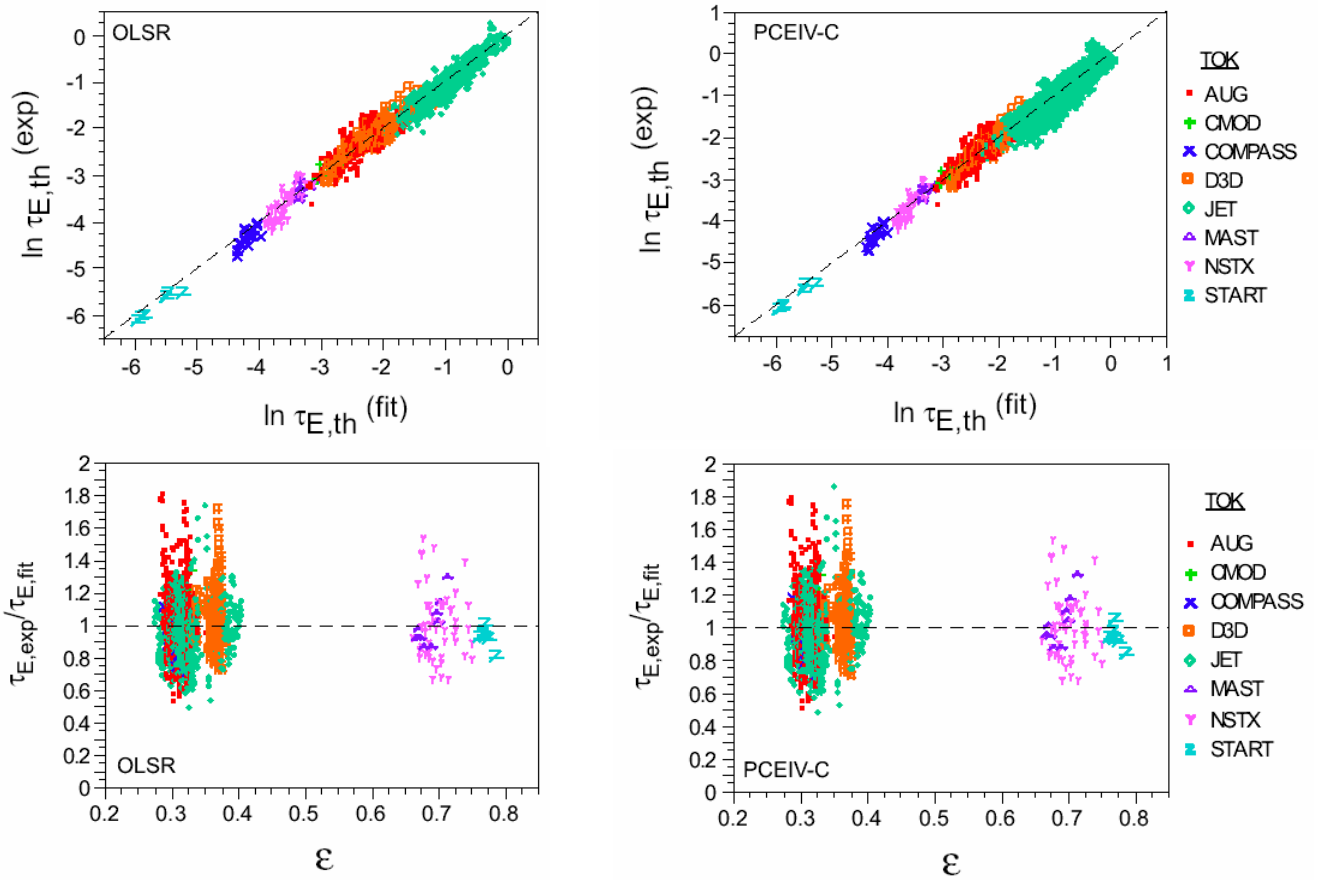


Fig. 3 Scalings based on the engineering variable predictor set for OLSR (Case 1) and PCEIV-C (Case 3). Top panels show the experimental vs fitted confinement times, while the bottom panels show the confinement time enhancements vs ϵ .

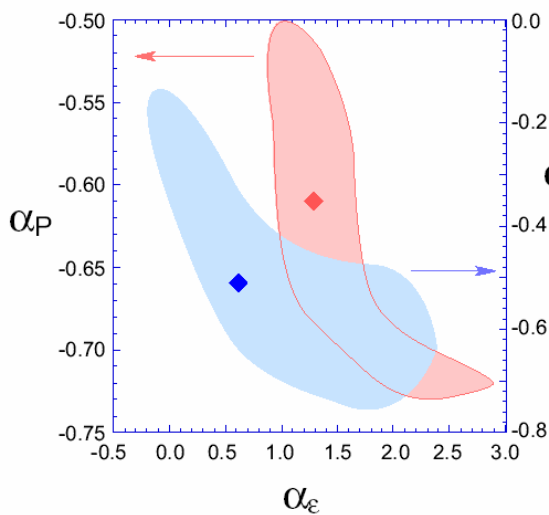


Fig. 4 Range of exponents for power (red) and β (blue) as a function of ϵ from error analysis based on the PCEIV method. The β - ϵ exponent (α_β , α_ϵ) range is transformed from the power- ϵ (α_p , α_ϵ) range.

External Distribution

Plasma Research Laboratory, Australian National University, Australia
Professor I.R. Jones, Flinders University, Australia
Professor João Canalle, Instituto de Fisica DEQ/IF - UERJ, Brazil
Mr. Gerson O. Ludwig, Instituto Nacional de Pesquisas, Brazil
Dr. P.H. Sakanaka, Instituto Fisica, Brazil
The Librarian, Culham Science Center, England
Mrs. S.A. Hutchinson, JET Library, England
Professor M.N. Bussac, Ecole Polytechnique, France
Librarian, Max-Planck-Institut für Plasmaphysik, Germany
Jolan Moldvai, Reports Library, Hungarian Academy of Sciences, Central Research
Institute for Physics, Hungary
Dr. P. Kaw, Institute for Plasma Research, India
Ms. P.J. Pathak, Librarian, Institute for Plasma Research, India
Dr. Pandji Triadyaksa, Fakultas MIPA Universitas Diponegoro, Indonesia
Professor Sami Cuperman, Plasma Physics Group, Tel Aviv University, Israel
Ms. Clelia De Palo, Associazione EURATOM-ENEA, Italy
Dr. G. Grosso, Istituto di Fisica del Plasma, Italy
Librarian, Naka Fusion Research Establishment, JAERI, Japan
Library, Laboratory for Complex Energy Processes, Institute for Advanced Study,
Kyoto University, Japan
Research Information Center, National Institute for Fusion Science, Japan
Professor Toshitaka Idehara, Director, Research Center for Development of Far-Infrared Region,
Fukui University, Japan
Dr. O. Mitarai, Kyushu Tokai University, Japan
Mr. Adefila Olumide, Ilorin, Kwara State, Nigeria
Dr. Jiangang Li, Institute of Plasma Physics, Chinese Academy of Sciences, People's Republic of China
Professor Yuping Huo, School of Physical Science and Technology, People's Republic of China
Library, Academia Sinica, Institute of Plasma Physics, People's Republic of China
Librarian, Institute of Physics, Chinese Academy of Sciences, People's Republic of China
Dr. S. Mirnov, TRINITI, Troitsk, Russian Federation, Russia
Dr. V.S. Strelkov, Kurchatov Institute, Russian Federation, Russia
Kazi Firoz, UPJS, Kosice, Slovakia
Professor Peter Lukac, Katedra Fyziky Plazmy MFF UK, Mlynska dolina F-2, Komenskeho Univerzita,
SK-842 15 Bratislava, Slovakia
Dr. G.S. Lee, Korea Basic Science Institute, South Korea
Dr. Rasulkhozha S. Sharafiddinov, Theoretical Physics Division, Institute of Nuclear Physics, Uzbekistan
Institute for Plasma Research, University of Maryland, USA
Librarian, Fusion Energy Division, Oak Ridge National Laboratory, USA
Librarian, Institute of Fusion Studies, University of Texas, USA
Librarian, Magnetic Fusion Program, Lawrence Livermore National Laboratory, USA
Library, General Atomics, USA
Plasma Physics Group, Fusion Energy Research Program, University of California at San Diego, USA
Plasma Physics Library, Columbia University, USA
Alkesh Punjabi, Center for Fusion Research and Training, Hampton University, USA
Dr. W.M. Stacey, Fusion Research Center, Georgia Institute of Technology, USA
Director, Research Division, OFES, Washington, D.C. 20585-1290

The Princeton Plasma Physics Laboratory is operated
by Princeton University under contract
with the U.S. Department of Energy.

Information Services
Princeton Plasma Physics Laboratory
P.O. Box 451
Princeton, NJ 08543

Phone: 609-243-2750
Fax: 609-243-2751
e-mail: pppl_info@pppl.gov
Internet Address: <http://www.pppl.gov>